Geophysical Journal International

Advancing Astronomy and Geophysics

doi: 10.1093/gji/ggaa549

Geophys. J. Int. (2021) 224, 1658–1669 Advance Access publication 2020 November 17 GJI Seismology

A viscoelastic model for seismic attenuation using fractal mechanical networks

Guangchi Xing ¹ and Tieyuan Zhu ¹,2

¹Department of Geosciences, The Pennsylvania State University, University Park, PA 16802, USA. E-mail: gux8@psu.edu

Accepted 2020 November 13. Received 2020 October 11; in original form 2020 June 25

SUMMARY

Seismic attenuation (quantified by the quality factor O) has a significant impact on the seismic waveforms, especially in the fluid-saturated rocks. This dissipative process can be phenomenologically represented by viscoelastic models. Previous seismological studies show that the O value of Earth media exhibits a nearly frequency-independent behaviour (often referred to as constant-Q in literature) in the seismic frequency range. Such attenuation can be described by the mathematical Kjartansson constant-Q model, which lacks of a physical representation in the viscoelastic sense. Inspired by the fractal nature of the pore fluid distribution in patchy-saturated rocks, here we propose two fractal mechanical network (FMN) models, that is, a fractal tree model and a quasi-fractal ladder model, to phenomenologically represent the frequency-independent Q behaviour. As with the classic viscoelastic models, the FMN models are composed of mechanical elements (spring and dashpots) arranged in different hierarchical patterns. A particular parametrization of each model can produce the same complex modulus as in the Kjartansson model, which leads to the constant-Q. Applying the theory to several typical rock samples, we find that the seismic attenuation signature of these rocks can be accurately represented by either one of the FMN models. Besides, we demonstrate that the ladder model in particular exhibits the realistic multiscale fractal structure of the saturated rocks. Therefore, the FMN models as a proxy could provide a new way to estimate the microscopic rock structure property from macroscopic seismic attenuation observation.

Key words: Elasticity and anelasticity; Microstructure; Fractals and multifractals; Seismic attenuation; Wave propagation.

1 INTRODUCTION

The seismic attenuation phenomenon is caused by the energy loss during the propagation of seismic waves in the Earth. Many mechanisms have been proposed to account for the loss, among which the presence of the porous fluid appears to be a major cause. Among this group, the wave-induced fluid flow (WIFF) mechanism is commonly accepted, where the pressure gradients generated by the passing seismic waves give rise to viscous fluid flow accompanied by internal friction (Müller *et al.* 2010). Besides, given that the seismic attenuation could also be attributed to the relaxation of the highly viscous fluid in the isolated pores (Wang *et al.* 2017), it is reasonable to phenomenologically represent seismic attenuation using viscoelastic models (Borcherdt 2009). Generally, these viscoelastic models, also known as mechanical (rheological) models, consist of springs and dashpots, where the spring exhibits the elastic property, while the dashpot represents the viscous nature. Simple combinations of springs and dashpots lead to classic mechanical element models including the Maxwell model, the Kelvin–Voigt model, and the Zener (standard linear solid, SLS) model, all of which correspond to specific dissipation and dispersion patterns over different frequencies. A detailed review of these models can be found in Carcione (2007).

In seismology, the quality factor Q is used to quantify the seismic attenuation. A lower Q value corresponds to stronger attenuation, which has significant impacts on seismic waveform by reducing its amplitude and distorting its shape. It has been observed in lab experiments and *in situ* measurements (e.g. McDonal *et al.* 1958; Knopoff 1964) that the attenuation factor varies almost linearly with frequency, that is, Q is frequency-independent (constant), in the seismic frequency band. Although the frequency-dependent Q phenomenon has been proposed in some other studies (e.g. Sams *et al.* 1997; Molyneux & Schmitt 2000; Adam *et al.* 2009; Borgomano *et al.* 2017), the simple frequency-independent Q model (often referred to as constant-Q in literature) has been commonly used in practical applications including seismic wavefield simulation and seismic imaging (e.g. Carcione *et al.* 2002; Zhu *et al.* 2014).

²EMS Energy Institute, The Pennsylvania State University, University Park, PA 16802, USA

This frequency-independent Q behaviour, however, cannot be represented by a single mechanical element model (e.g. the SLS model) since all the models of this type produce a frequency-dependent Q. To fit the observation, a distribution of mechanical elements characterized by different relaxation times are superposed in parallel to achieve an approximate constant-Q within a limited frequency band. The relaxation time of each mechanical element is determined via a curve-fitting process. This type of models, known as nearly constant-Q models, include the generalized standard linear solid model (GSLS, e.g. Carcione $et\ al.\ 1988$; Morozov & Deng 2016) and the generalized Maxwell body (GMB, e.g. Emmerich & Korn 1987), both of which have been widely used for seismic wave simulation. Besides these mechanical models, the constant-Q behaviour can be captured by an elegant mathematical model proposed by Kjartansson (1979) for all the frequencies. This Kjartansson formulation requires only a limited number of parameters without the need for a relaxation time spectrum. This model leads to a concise viscoelastic wave equation (e.g. Carcione $et\ al.\ 2002$; Zhu & Harris 2014; Zhu & Carcione 2014) with the aid of the fractional derivative technique (Caputo 1967), which can improve the efficiency of seismic wave numerical simulation and imaging (e.g., Zhu $et\ al.\ 2014$; Xing & Zhu 2019). In the medical imaging community, a generic spring-dashpot model known as the Maxwell–Wiechert model is widely used because it can represent the viscoelastic response of any materials (Näsholm & Holm 2013; Holm 2019). Theoretically, it could potentially provide a spring-dashpot equivalent of the Kjartansson model, which has a fractional formulation in time domain, with infinite parallel branches of mechanical elements (Näsholm & Holm 2011; Holm 2018).

Seismic attributes like attenuation as well as its associated velocity dispersion are sensitive to the microscopic geometry of porous rocks, especially to the distribution pattern of the porous fluid. For example, Cadoret *et al.* (1995) conducted laboratory experiments to argue that even at the same saturation level, drainage and imbibition produce different pore fluid distributions, which further lead to different attenuation. Such dependency of attenuation on fluid distribution has also been confirmed by theoretical studies based on the Biot theory (Gurevich & Lopatnikov 1995; Müller & Gurevich 2004; Toms *et al.* 2006). Interestingly, several laboratory observations (Engelberts *et al.* 1951; Feder 1988) pointed out that the pore fluid distribution in patchy-saturated rocks exhibits a fractal nature (Engelberts *et al.* 1951; Feder 1988). Based on the fractal pore fluid distribution, Müller *et al.* (2008) numerically predict the variation of the velocity–saturation relation between the Gassmann–Wood and Gassmann–Hill bounds depending on a fractal property, that is, the Hurst exponent. Given that the assumption of a fractal pore fluid distribution is supported by these studies, we are motivated to investigate if we can develop a spring-dashpot model with a fractal structure to phenomenologically represent the frequency-independent *Q* seismic attenuation, that is, to physically represent the mathematical Kjartansson model. Such a model could potentially serve as a proxy to bridge the gap between the macroscopic attenuation phenomenon and the microscopic rock structure to improve our understanding of the attenuation mechanism, and further shed light upon the estimation of microscopic geometries from seismic observations.

In this paper, we propose a type of mechanical models, that is, the fractal mechanical network (FMN) models, including a fractal tree model (FTM) and a quasi-fractal ladder model (QLM), to describe the seismic attenuation behaviour of fractal porous rocks. Both of them are phenomenological viscoelastic models that consist of springs and dashpots arranged in different hierarchical patterns. Similar models were reported by Heymans & Bauwens (1994) to describe the viscoelastic behaviour of polymers. We here reformulate the FTM and the QLM to capture the frequency-independent Q of rocks. Then we investigate whether both models can produce the Kjartansson frequency-independent Q constitutive relation and demonstrate using four typical rocks as examples. Finally, we explore the significance of the FMN models in relating the seismic attenuation to the fractal structure of porous media.

This paper is organized as follows. We start by reviewing the Kjartansson frequency-independent *Q* model. Next, we describe the FMN models and illustrate the application on several typical rocks. Following that, we discuss some differences between the two proposed FMN models and demonstrate their potential in bridging the macroscopic phenomenon and microscopic structure.

2 KJARTANSSON FREQUENCY-INDEPENDENT Q MODEL

Kjartansson (1979) proposed an elegant causal model that describes the frequency-independent Q viscoelastic behaviour of the rocks with a few parameters. It formulates the frequency-domain complex modulus M for the angular frequency ω as:

$$M(\omega) = M_0 \left(\frac{i\omega}{\omega_0}\right)^{2\gamma},\tag{1}$$

where ω_0 is the reference angular frequency, M_0 is a real parameter with the dimension of bulk modulus and γ is a dimensionless parameter that describes the strength of attenuation as well as how significant the attenuation-associated effects vary for different frequencies. The quality factor Q is defined as the ratio between the real and imaginary parts of the complex modulus:

$$Q = \frac{\Re\{M\}}{\Im\{M\}} = \frac{1}{\tan(\pi\gamma)},\tag{2}$$

where Q is not a function of ω , so the Kjartansson model produces an analytical frequency-independent Q.

This complex modulus characterizing the constitutive relation in frequency domain, associated with the conservation of mass and momentum, leads to a complex wavenumber $k(\omega) = \sqrt{\frac{\rho}{M(\omega)}}\omega$, where ρ denotes the density. The real and imaginary parts of this wavenumber govern two attenuation-associated effects, that is, the phase velocity dispersion and the amplitude decay, respectively. In particular, the phase velocity c_p and the attenuation factor α for each angular frequency ω are derived as:

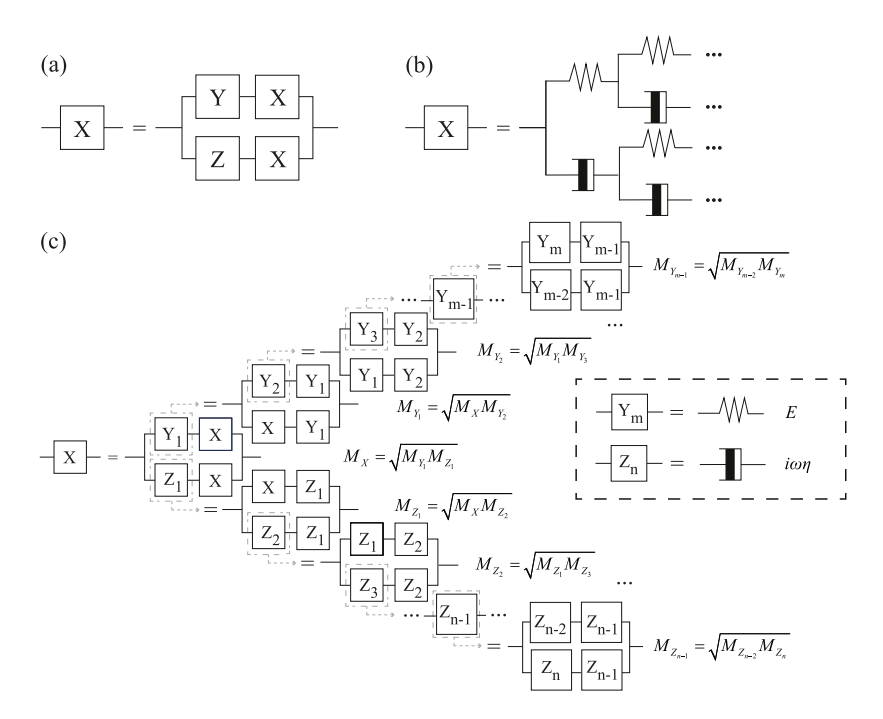


Figure 1. (a) An elementary FTM; (b) an explicit example of (a) when *Y* is a spring and *Z* is a dashpot; (c) the structure of the FTM with the inset showing the two end-member models; each equation expresses the complex modulus of the corresponding mechanical element by calling eq. (7). The equal signs in all the subfigures denote that a detailed structure of the left-hand side is the right-hand side.

$$c_p(\omega) = \frac{\omega}{\Re\{k(\omega)\}} = c_0 \left(\frac{\omega}{\omega_0}\right)^{\gamma},\tag{3}$$

$$\alpha(\omega) = -\Im\{k(\omega)\} = \frac{\omega_0^{\gamma}}{c_0} \tan\left(\frac{\pi\gamma}{2}\right) \omega^{1-\gamma},\tag{4}$$

where $c_0 = \sqrt{\frac{M_0}{\rho}} \left(\cos\left(\frac{\pi\gamma}{2}\right)\right)^{-1}$ is the reference phase velocity corresponding to the reference angular frequency ω_0 . In practice, a reasonable Q > 3 gives a very small $\gamma < 0.1$. Thus, the attenuation factor (eq. 4) has an almost linear dependence on frequency, which was advocated by McDonal *et al.* (1958) to fit seismic attenuation measurements of Pierre Shale rocks.

The Kjartansson complex modulus (eq. 1) leads to a stress-strain constitutive relation characterized by a fractional derivative in the time domain:

$$\sigma(t) = M_0 \omega_0^{-2\gamma} \frac{\partial^{2\gamma}}{\partial t^{2\gamma}} \epsilon(t), \tag{5}$$

where σ is the stress and ϵ denotes the strain, and the fractional derivative is introduced by Caputo (1967). The fractional derivative in eq. (5) makes it less straightforward to represent the Kjartansson formulation with a spring-dashpot mechanical model, since the stresses of a spring and a dashpot are proportional to the strain and the first time derivative of the strain, respectively.

3 FRACTAL MECHANICAL NETWORK MODELS

In this section, we derive and show two FMN models (FTM and QLM) composed of springs and dashpots to physically represent the Kjartansson frequency-independent Q.

3.1 Fractal tree model

We start from an introductory model as shown in Fig. 1(a), where a mechanical element X with a recursive structure is connected to arbitrary elements Y and Z. This model is considered as a fractal model due to its self-similarity since the whole model X is identical to the X's on both branches. For example, when Y is a spring and Z is a dashpot, the model X becomes a fractal tree network (Heymans & Bauwens 1994), as shown in Fig. 1(b). When two mechanical elements are connected in parallel, the total equivalent complex modulus equals to the sum of the complex moduli of both elements; the equivalent complex modulus for serial connection equals to the reciprocal of sum of the reciprocal complex moduli. Hence, for arbitrary elements Y and Z, the complex modulus of X (denoted by M_X) can be mathematically represented by

$$M_X = \frac{1}{\frac{1}{M_Y} + \frac{1}{M_X}} + \frac{1}{\frac{1}{M_Z} + \frac{1}{M_X}},\tag{6}$$

Table 1. Parameters related to the FTM for different rock samples.

| Rock type | $c_p (\mathrm{km} \mathrm{s}^{-1})$ | $\alpha (\mathrm{km}^{-1})$ | $\rho (\mathrm{g} \mathrm{cm}^{-3})$ | Q | m | n | E (GPa) | η (mPa·s) | $Q_{\rm FTM}$ |
|-------------------------|---------------------------------------|------------------------------|--|-------|----|-----|---------|-----------|---------------|
| Granite (Quincy, MA) | 5.00 | 0.210 | 2.53 | 149.6 | 1 | 234 | 70.43 | 2.40 | 149.6 |
| Basalt (Painesdale, MI) | 5.50 | 0.414 | 2.62 | 69.0 | 5 | 537 | 100.38 | 2.40 | 69.0 |
| Shale (Pierre, CO)* | 2.06 | 2.421 | 1.93 | 31.5 | 2 | 97 | 13.19 | 2.40 | 31.5 |
| Sandstone (Navajo) | 4.00 | 1.770 | 2.39 | 22.2 | 19 | 644 | 79.09 | 2.40 | 22.2 |

^{*}The data for the shale are revised according to McDonal et al. (1958) and Wuenschel (1965).

where M_Y and M_Z are the complex moduli of their corresponding mechanical elements, respectively. Manipulation of eq. (6) gives the overall modulus M_X as the geometric mean of M_Y and M_Z :

$$M_X = \sqrt{M_Y M_Z}. (7)$$

Moreover, the elements Y and Z can have similar fractal structure as well. By recursively applying this elementary architecture (Fig. 1a), an FTM can be constructed as shown in Fig. 1(c). The hierarchical fractal structures extend to m-1 levels on one branch and n-1 on the other. We define the end-member elements by letting Y_m be a spring with a Young's modulus E, and Z_n be a dashpot with a viscosity η (Fig. 1c, inset). Thus their corresponding complex moduli M_{Y_m} and M_{Z_n} are E and $i\omega\eta$, respectively. By recursively using the property in eq. (7), we obtain the complex modulus of the entire model:

$$M_X = M_{Y_m}^{\frac{n}{m+n}} M_{Z_n}^{\frac{m}{m+n}} = (E^{\frac{n}{m+n}} \eta^{\frac{m}{m+n}})(i\omega)^{\frac{m}{m+n}}.$$
 (8)

Comparing eq. (8) to the complex modulus of the Kjartansson model (eq. 1), we find out that they have similar expressions. In particular, for any rational number 2γ , we can find a combination of integers m and n such that

$$2\gamma = \frac{m}{m+n}. (9)$$

And if 2γ is irrational, we can always use rational numbers to approximate it given a specific accuracy. Then, assigning appropriate values for E and η that satisfy

$$M_0 \omega_0^{-2\gamma} = E^{\frac{n}{m+n}} \eta^{\frac{m}{m+n}} \tag{10}$$

leads to the equivalence between eqs (8) and (1). Therefore, for any rock that satisfies the mathematical frequency-independent Q formulation, we can always find a specific mechanical FTM that produces the same modulus.

To test the theory, we investigate the FTMs corresponding to four particular rocks (granite, basalt, shale and sandstone) as shown in Table 1. The first three columns of Table 1 show some relevant characteristics, including the rock type, the phase velocity and the attenuation factor measured at 50 Hz, of four different rocks from a data set compiled by Dobrin & Savit (1988). Based on these parameters, we calculate the density with the empirical Nafe–Drake relation (Brocher 2005) and compute the Q value using $Q = \pi f/\alpha c_n$.

We assume that the phase velocity c_p , the attenuation factor α , the density ρ and the quality factor Q are known. For each rock sample, the Q value is used to calculate γ based on eq. (2). The γ is then plugged into eq. (9) to find the proper integers m and n. In this process, we restrict the denominator of the right-hand side of eq. (9) to be less than 1000, which turns out to give enough accuracy. In another word, we find integers m and n, the sum of which is less than 1000, so that the error of eq. (9) is minimized. The resultant m and n are listed in Table 1. The choice of Young's modulus E and viscosity η is not unique as long as the condition in eq. (10) is met. In this study, the bulk viscosity of water, that is, 2.40 mPa·s (Dukhin & Goetz 2009), is assigned to η and E is then calculated using eq. (10). Thus, for each rock sample, a corresponding FTM is determined by a set of parameters (m, n, E, η) , which are listed in the 6th–9th columns in Table 1. For the validation, these parameters are plugged into eq. (8) to compute the complex moduli, and the modelled Q values (Q_{FTM}) are obtained according to the first part of eq. (2). The resultant Q values are listed in the last column of Table 1. As it turns out, the modelled Q_{FTM} is identical to the ground truth Q for each sample.

3.2 Quasi-fractal ladder model

In addition to the FTM, we develop a second fractal model, that is, the QLM. Below, we introduce the structure of the QLM based on the continued fraction theory (Jones & Thron 1980), and then discuss its connections to porous rocks.

As with the FTM (e.g., Fig. 1b), the QLM is also an infinite model. Yet to better illustrate its properties, we show in Fig. 2, a finite version of the QLM. The QLM has 'super-dashpots' on the rungs and 'super-springs' on one of the struts. In particular, each super-spring/super-dashpot is made up of a number of springs/dashpots connected in parallel. Thus, the integrated Young's modulus E_k of the super-spring is the summation of its corresponding springs; similarly, the integrated viscosity η_k of the super-dashpot is the summation of its corresponding dashpots. The 'quasi-fractal' refers to the fact that this model, unlike the FTM, is not self-similar because the attributes (either integrated Young's modulus or integrated viscosity) of the super-springs/super-dashpots are distinct from each other. The finite QLM in Fig. 2 has the complex modulus:

$$M = \frac{E_1}{1+} \frac{(i\omega\eta_1)^{-1} E_1}{1+} \frac{(i\omega\eta_1)^{-1} E_2}{1+} \frac{(i\omega\eta_2)^{-1} E_2}{1+} \frac{(i\omega\eta_2)^{-1} E_3}{1+} \dots \frac{(i\omega\eta_{n-2})^{-1} E_{n-1}}{1+} \frac{(i\omega\eta_{n-1})^{-1} E_{n-1}}{1+} \frac{(i\omega\eta_{n-1})^{-1} E_n}{1+},$$
(11)

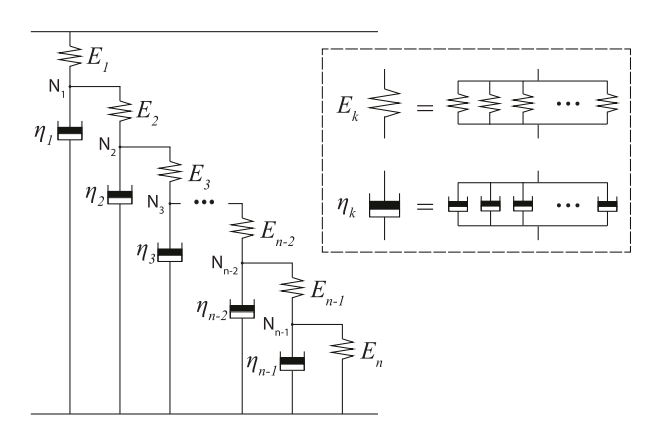


Figure 2. The structure of the finite QLM. The building blocks of the QLM are super-springs and super-dashpots, which are composed of a number of springs and dashpots connected in parallel, respectively (inset).

where the notation of the continued fraction is:

$$\frac{a_1}{b_1 + \frac{a_2}{b_2 + \frac{a_3}{b_3 + \dots}} \dots = \frac{a_1}{b_1 + \frac{a_3}{b_2 + \frac{a_3}{b_2 + \dots}}}.$$

A detailed derivation of eq. (11) can be found in Appendix A. As $n \to \infty$, the infinite QLM yields the following expression:

$$\frac{M}{E_1} = \frac{1}{1+} \frac{(i\omega\eta_1)^{-1} E_1}{1+} \frac{(i\omega\eta_1)^{-1} E_2}{1+} \frac{(i\omega\eta_2)^{-1} E_2}{1+} \frac{(i\omega\eta_2)^{-1} E_3}{1+} \frac{(i\omega\eta_3)^{-1} E_3}{1+} \dots$$
(12)

Recalling the continued fraction theory (Jones & Thron 1980), for a complex number z and a real number β , we have

$$(1+z)^{\beta} = \frac{1}{1+} \frac{-\beta z}{1+} \frac{\frac{1(1+\beta)z}{1+2}}{1+} \frac{\frac{1(1-\beta)z}{2+3}}{1+} \frac{\frac{2(2+\beta)z}{3+4}}{1+} \frac{\frac{2(2-\beta)z}{4+5}}{1+} \dots$$
(13)

A detailed explanation of eq. (13) can be found in Appendix B. The right-hand side of eq. (13) appears to have a similar form to that of eq. (12). Given an arbitrary large value b, the effect of which will be shown later, we let $z = \frac{b}{i\omega}$. When the attributes of the super-springs and of the super-dashpots satisfy

$$\eta_1 = -\frac{E_1}{b\beta},\tag{14}$$

$$E_{k} = \eta_{k-1} \cdot b \cdot \frac{(k-1)(k-1+\beta)}{(2k-3)(2k-2)}, \qquad (k=2,3,4...)$$

$$\eta_{k} = E_{k} \cdot \frac{1}{b} \cdot \frac{(2k-2)(2k-1)}{(k-1)(k-1-\beta)}, \qquad (k=2,3,4...)$$
(15)

$$\eta_k = E_k \cdot \frac{1}{b} \cdot \frac{(2k-2)(2k-1)}{(k-1)(k-1-\beta)}, \qquad (k=2,3,4...)$$
(16)

each term on the right-hand side of eq. (12) is equivalent to its counterpart of eq. (13). Hence, the complex modulus M of the QLM becomes

$$M = E_1 \left(1 + \frac{b}{i\omega} \right)^{\beta}. \tag{17}$$

Given a frequency range of interest, we can always find an appropriate b such that $|\frac{b}{ba}| \gg 1$. Then, the QLM complex modulus (eq. 17) can be approximated by

$$M(\omega) \approx E_1 b^{\beta} (i\omega)^{-\beta},$$
 (18)

where the approximation can be achieved for any given accuracy. Thus, eq. (18) becomes the Kjartansson formulation (eq. 1) by assigning

$$\beta = -2\gamma,\tag{19}$$

$$E_1 = M_0 \omega_0^{-2\gamma} b^{2\gamma}. \tag{20}$$

Therefore, a rock with the frequency-independent Q can be represented by a QLM given a specific accuracy. The related parameters are determined by eqs (19) and (20) and (14)-(16). Similar ladder models have been proposed to describe the viscoelastic behaviour at low frequencies (Strick & Mainardi 1982; Strick 1984; Schiessel & Blumen 1993). Different from them, by introducing the auxiliary parameter b, our QLM can approximate the frequency-independent Q behaviour accurately for any frequency of interest.

We take the rock samples in Table 1 as examples to evaluate the performance of the QLM. We consider the seismic frequency range of 1–200 Hz and choose a proper $b=10^6$. Each rock sample is characterized by phase velocity c_p , attenuation factor α , density ρ and Q value. These properties are converted into Kjartansson parameters (M_0, ω_0, γ) , which are further used to calculate the integrated Young's modulus of each super-spring and the integrated viscosity of each super-dashpot using eqs (19) and (20) and (14)–(16). The results are shown in Fig. 3.

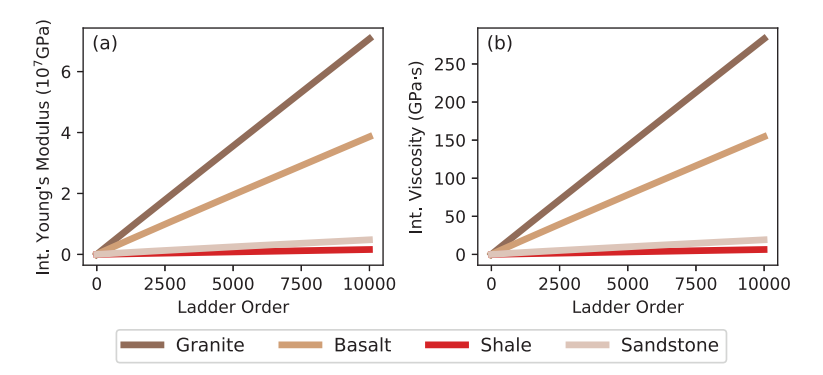


Figure 3. (a) Integrated Young's modulus E_k of each super-spring and (b) integrated viscosity η_k of each super-dashpot as functions of ladder order k in the QLM for four rock samples in Table 1.

It turns out that the values of both super-springs (integrated Young's modulus) and super-dashpots (integrated viscosity) increase almost linearly with the ladder order k. To interpret these patterns, we take the integrated Young's modulus as an example (the integrated viscosity pattern can be explained similarly). Manipulation of eqs (15) and (16) yields a recursive relation:

$$\frac{E_{k+1}}{E_k} = \frac{k+\beta}{k-1-\beta} \approx \frac{k}{k-1} \qquad (k=2,3,4\ldots).$$
 (21)

This approximation is valid because β is a small value ($|\beta| \ll 0.2$) for low loss media ($Q \gg 3$). And it becomes more and more accurate as the ladder order k increases. Thus, the recursion of eq. (21) gives the relation between the integrated Young's modulus and the ladder order:

$$E_{k+1} \approx \frac{k}{k-1} E_k \approx \frac{k}{k-2} E_{k-1} \approx \dots \approx k E_2. \tag{22}$$

Hence, the sequence $\{E_k\}$ is almost linear, and the slope of the integrated Young's modulus (Fig. 3) is determined by the value of E_2 . We can estimate E_2 (the approximate slope) from eqs (14), (15), (19) and (20):

$$E_2 = \frac{1 - 2\gamma}{4\gamma} M_0 \omega_0^{-2\gamma} b^{2\gamma} \approx \frac{1 - 2\gamma}{4\gamma} M_0, \tag{23}$$

as $\omega_0^{-2\gamma}b^{2\gamma}\approx 1$ for the small values of γ . Qualitatively, a larger Q leads to a smaller γ and thus a larger E_2 ; meanwhile, a larger modulus M_0 due to higher phase velocity or density gives a larger E_2 as well. Hence, a steeper slope is attributed to either a higher Q value (e.g. the granite has the largest slope since it has a higher Q than the other samples) or a higher modulus (e.g. compared to the shale, the sandstone has a smaller Q but a higher modulus, which leads to a relatively larger slope). Note that the number of springs/dashpots in each super-spring/super-dashpot in the QLM is theoretically arbitrary, so the attributes (Young's modulus or viscosity) of the springs/dashpots can be casted into any realistic values.

The complex modulus of the whole model is obtained by eq. (17) for each rock sample. Based on these moduli, we compute the QLM-modelled Q values, phase velocities and attenuation factors for all the frequencies according to the first parts of the eqs (2)–(4), respectively. Also, the corresponding FTM-modelled attributes are predicted via eq. (8). As shown in Figs 4(a)–(c), the theoretical Kjartansson curves and the predicted curves (both FTM-modelled and QLM-modelled) agree with each other for all the attributes of all the rock samples. Using the shale sample as an example, we show in Figs 4(d)–(f), the residual between the predicted and the theoretical curves for all the attributes, all of which are less than 3 orders smaller than the original values. Furthermore, we extract the dispersion curves for the shale sample and compare them with the *in situ* measurement of the Pierre Shale (McDonal *et al.* 1958; Wuenschel 1965). As shown in Fig. 5, the data fit very well with not only the theoretical but also the modelled curves. Thus, these validations demonstrate the capability of the QLM, as well as the FTM, to physically represent the Kjartansson frequency-independent Q formulation.

The importance of the selection of b is discussed by particularly investigating the shale sample in Table 1. We simulate the Q values for the seismic frequency range (1–200 Hz) based on the QLM with various choices of b, and show the results in Fig. 6(a). The approximation in eq. (18) requires $|\frac{b}{i\omega}| \gg 1$. For a fixed b, the modelling of the low-frequency part will be more accurate than the high-frequency part, as confirmed in Fig. 6(a). Hence, for a given frequency range of interest, we can always have a big enough b to maintain a constant b0 over the entire band.

In addition, Figs 6(b) and 6(c) show the modelled Q values using finite QLMs with various choices of n and b. We found that the finite model can also give a frequency-independent Q accurately with proper n and b. Note that a larger b requires a larger n to make the finite model converge to the infinite limit. This argument is confirmed by the fact that $n = 10^3$ yields a good approximation for $b = 10^5$, while it produces large errors for $b = 10^7$.

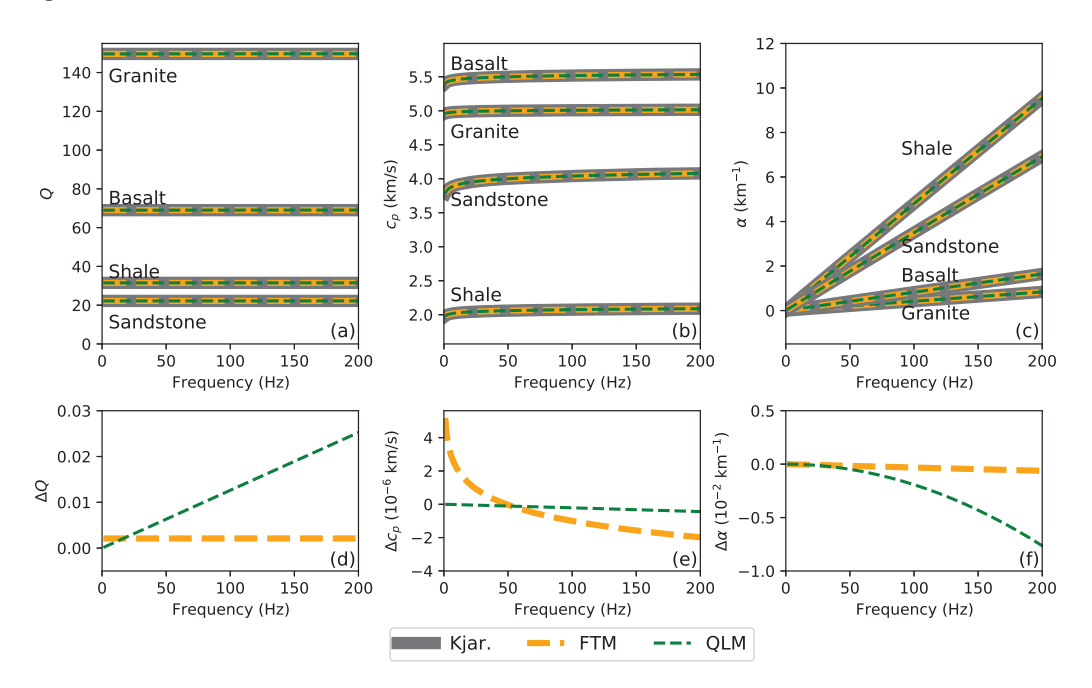


Figure 4. (a) Q value, (b) phase velocity c_p and (c) attenuation factor α computed using the theoretical Kjartansson model (Kjar., thick grey solid lines), the FTM (orange dashed lines) and the QLM (thin green dashed lines) for the rock samples in Table 1. To better visualize the residual, we take the shale sample as an example, and show the residual (compared to the reference Kjartansson model) of both FTM and QLM for (d) quality factor residual ΔQ , (e) phase velocity residual Δc_p and (f) attenuation factor residual $\Delta \alpha$.

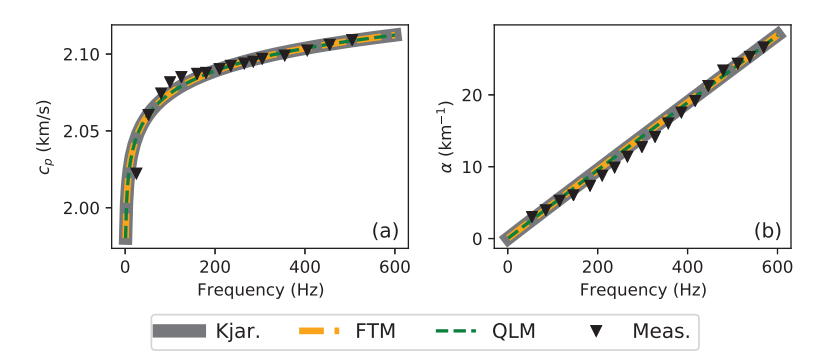


Figure 5. The comparison of (a) phase velocity c_p and (b) attenuation factor α between the theoretical Kjartansson model (Kjar., thick grey solid lines), the FTM (orange dashed lines), the QLM (thin green dashed lines) and the *in situ* measurement (black triangles) for the Pierre Shale rock sample.

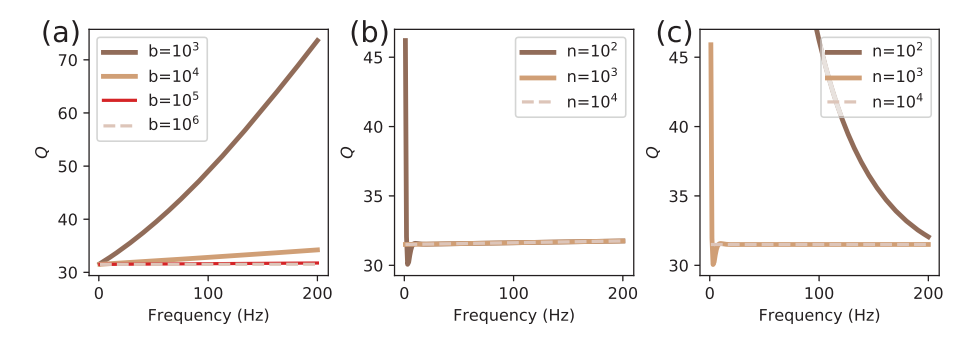


Figure 6. (a) Q values modelled by infinite QLMs, where different lines represent different b values (see the legend); (b) Q values modelled by finite QLMs with $b = 10^5$, where different lines represent different numbers of hierarchical layers n (see the legend); (c) Q values modelled by finite QLMs with $b = 10^7$, where different lines denote different numbers of hierarchical layers n (see the legend). Note that in (c), the curve for $n = 10^2$ has a huge error for low frequencies and goes beyond the limit of the figure.

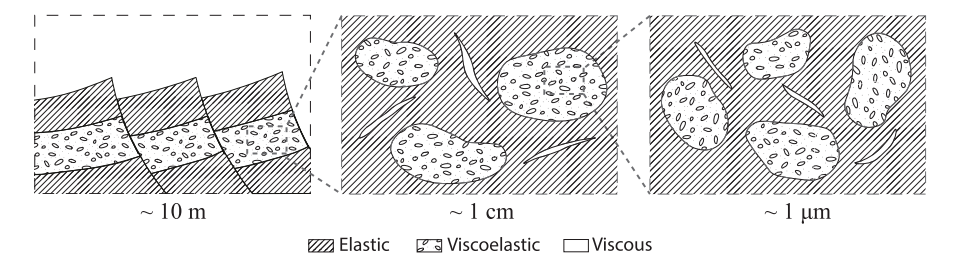


Figure 7. A sketch illustration of the multiscale structure of porous rocks with patchy saturation.

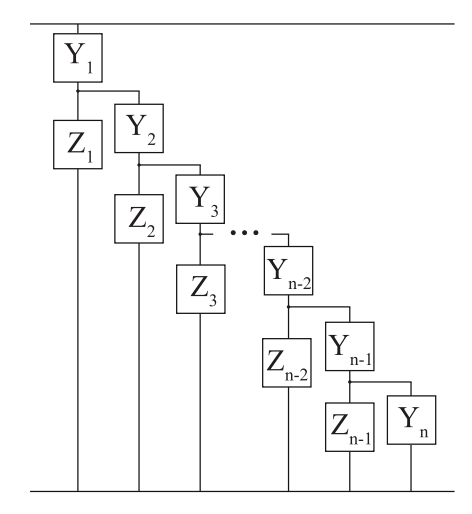


Figure 8. The structure of the finite generalized QLM.

4 DISCUSSION

We have shown that both the FTM and the QLM can accurately model the frequency-independent Q attenuation characteristic of seismic waves propagating in subsurface rocks. There are several differences between these two phenomenological models. In terms of hierarchical patterns, the springs as well as the dashpots are identical in the FTM; while the QLM consists of elements (super-springs and super-dashpots) with various attributes. Previously, a fractal ladder model made up of identical springs and identical dashpots has been investigated by several authors (Heymans & Bauwens 1994; Kelly & McGough 2009) to describe the power-law absorption of materials such as biological tissues. But the derivation of their model restricts the power order to some specific values, which prevents the fractal ladder model from being generalized to represent the rock with an arbitrary Q. Moreover, the FTM is intrinsically infinite, while the QLM can be truncated into a finite QLM. As the number of ladder layers increases ($\sim 10^3$ in our example), the complex moduli of the finite QLM converges to the Kjartansson formulation. Thus, this finite QLM model can be potentially used for numerical simulation to investigate the microscopic behaviour of the rocks with the frequency-independent Q property.

Besides the identical phenomenological relaxation behaviour, the porous rocks have similar internal fractal structure as the FMNs, especially the QLM. On account of the fractal nature (Engelberts *et al.* 1951; Feder 1988), a schematic of porous rocks with a multiscale structure is shown in Fig. 7. It has a hierarchical structure made up of components with different elastic/viscous properties. At the geological scale (~ 10 m), the unsaturated layers alternate with saturated ones due to various permeabilities and porosities. The former are modelled as elastic matrices, while the latter are regarded as viscoelastic. A microscopic view of the saturated rocks (~ 1 cm) reveals the fractures filled with viscous fluid, the viscoelastic saturated patches, and the surrounding elastic rock frames. A close-up of the viscoelastic part exhibits a similar structure and such an arrangement continues down to the pore scale ($\sim 1 \mu m$). This multiscale structure has a remarkable correspondence with the topology of the QLM (Fig. 2): at each scale level, the elastic rock frame and the viscous fluid in Fig. 7 can be represented by a super-spring and a super-dashpot in Fig. 2, respectively. Such a microscopic correspondence, along with the macroscopic consistency, suggests the significance of the QLM to physically describe the porous rocks.

Yet the multiscale model (Fig. 7) is an idealized heuristic model. To be realistic, the components at each level are not likely to be either purely elastic or purely viscous as the QLM suggests (Fig. 2). Instead, a realistic scenario is that the porous rock is saturated by two (or more) immiscible fluids (Müller *et al.* 2010), and the resultant patches saturated by different fluids have different viscoelastic properties. The topology of such a patchy saturation model with fractal fluid distribution can be represented by a generalized QLM (GQLM, Fig. 8). Compared to the QLM (Fig. 2), the sequences of super-springs and super-dashpots are generalized into two sequences of viscoelastic elements $\{Y_k\}$ and $\{Z_k\}$ ($k = 1, 2, 3, \ldots$). We demonstrate (in Appendix C) that when $\{Y_k\}$ are constant-Q elements with a high Q value and $\{Z_k\}$ with a low Q, the entire GQLM can produce the frequency-independent Q behaviour. Hence, the GQLM can represent the realistic multiscale

patchy-saturated media: at each scale level (index k), there exist high-Q areas (represented by Y_k) dominated by one porous fluid, low-Q areas (represented by Z_k) dominated by another porous fluid, and the areas with the mixture of these two.

In addition to the phenomenological models, the quantitative analysis of the WIFF mechanism has been conducted based on the Biot theory of poroelasticity (Biot 1956a, b, 1962) for heterogeneous porous media with different complexities, including 1-D regular (e.g. White et~al.~1975), 3-D regular (e.g. White 1975), 1-D random (e.g. Müller & Gurevich 2004), 2-D random (e.g. Helle et~al.~2003) and 3-D random media (e.g. Müller & Gurevich 2005; Toms et~al.~2007). These studies can well explain the frequency-dependent Q. Nevertheless, if the fractal heterogeneity is taken into account, the poroelastic modelling gives rise to the asymptotic scaling $Q^{-1} \propto \omega^{-H}$ from both numerical simulations and analytical derivations (Shapiro & Müller 1999; Pride & Masson 2006; Müller et~al.~2008), where H is the Hurst exponent. In particular, $H \rightarrow 0$ indicates a rather fractal-like heterogeneity, which corresponds to our proposed FMN structures, and further leads to a frequency-independent Q. As we have discussed, the porous media represented by the FMN have fluid patches with a broad range of sizes in a fractal fashion. Consequently, as the viscoelastic deformation exists at various scopes for the FMN, the WIFF process in the porous rocks takes place at all length scales corresponding to different frequencies (Toms et~al.~2007; Müller et~al.~2008), which provides a conceptual interpretation of the frequency-independent Q behaviour.

The Kjartansson constitutive relation represented by the proposed FMNs results in a fractional derivative (eq. 5). A pioneering work by Scott-Blair (1949) proposed such a fractional relation that is intermediate between the behaviours of springs and dashpots. Koeller (1984) introduced an imaginary mechanical element 'springpot' (also referred to as Scott-Blair element/model in some literature, e.g. Mainardi & Spada 2011) to represent this fractional constitutive relation. As a result, replacing the springs or dashpots in the classic mechanical element models with the springpot produces new fractional models, such as the fractional Maxwell model (e.g. Stankiewicz 2018), the fractional Kelvin–Voigt model (e.g. Caputo *et al.* 2011), the most general fractional Zener model (e.g. Näsholm & Holm 2013; Metzler & Nonnenmacher 2003) and its special case the Cole–Cole model (e.g. Hanyga 2003; Picotti & Carcione 2017). These models have been utilized to study the viscoelastic behaviour of materials including biological tissues, polymers and gas-saturated rocks. Since our proposed FMN models can be considered as physical representation of a springpot, these fractional models can be represented by connecting the FMNs with proper springs and dashpots. Although the fractional models have more complicated structures than the original FMN models, they are more flexible to fit the data exhibiting frequency-dependent *Q* phenomenon. It is also noticeable that the frequency dependency of *Q* is often observed in a larger frequency band beyond the surface seismic frequency range, whereas the constant-*Q* is believed to be reasonable in a narrow-frequency bandwidth. We argue that this band-limited constant-*Q* could be naturally represented by a band-limited fractal model, such as the truncated finite QLM.

The importance of the FMN models lies in bridging the gap between the macroscopic attenuation phenomenon and the microscopic rock structure. On the one hand, because of the significant dependence of seismic attenuation on the fluid distribution pattern, small-scale heterogeneities should be taken into account for accurately seismic modelling, which will be computationally prohibitive (Sidler *et al.* 2013). To solve this problem, an upscaling process could be used to represent the heterogeneous media by equivalent phenomenological FMN models with lumped parameters. On the other hand, the macroscopic *Q* measurement could potentially indicate the microscopic fractal properties of a porous rock. Such indications could be conveyed via its corresponding FMN representation. Thus, how to establish a quantitative relation between the FMN models and the fractal characteristics of porous rocks should be investigated in the future.

5 CONCLUSION

We have presented two FMN models, that is, an FTM and a QLM. While these two models consist of springs and dashpots arranged in different hierarchical patterns, both of them can produce the same complex modulus as the Kjartansson model given an arbitrary accuracy. The new models phenomenologically simulate the frequency-independent Q seismic attenuation behaviour of the Earth media, and thus provide physical interpretations for the mathematical Kjartansson formulation. We validate the accuracy of the FMN models by applying to four rock samples, and all of them produce the expected attenuation behaviour. Moreover, we demonstrate that the QLM, in particular, can represent the multiscale structure of porous rocks. We conclude that the FMN models bridge the gap between the microscopic rock structure and the macroscopic attenuation phenomenon, and therefore provide a new way to determine the property of microscopic rock structure from seismic attenuation.

ACKNOWLEDGEMENTS

This work was supported by the National Energy Technology Laboratory of the U.S. Department of Energy under the U.S. DOE contract no. DE-FE0031544, and the National Science Foundation Grant EAR 1919650. The authors would like to thank Sven Peter Näsholm and an anonymous reviewer for their constructive comments.

DATA AVAILABILITY

The properties of rock samples are compiled from Dobrin & Savit (1988). The data of the Pierre Shale measurements are extracted from McDonal *et al.* (1958) and Wuenschel (1965).

REFERENCES

- Adam, L., Batzle, M., Lewallen, K. & van Wijk, K., 2009. Seismic wave attenuation in carbonates, J. Geophys. Res.: Solid Earth, 114(B6), doi.org/10.1029/2008JB005890.
- Biot, M., 1956a. Theory of elastic waves in a fluid-saturated porous solid. I. low frequency range, *J. Acoust. Soc. Am.*, **28**, 168–178.
- Biot, M.A., 1956b. Theory of propagation of elastic waves in a fluid-saturated porous solid. II. higher frequency range, *J. Acoust. Soc. Am.*, 28(2), 179–191.
- Biot, M.A., 1962. Mechanics of deformation and acoustic propagation in porous media, *J. Appl. Phys.*, **33**(4), 1482–1498.
- Borcherdt, R.D., 2009. Viscoelastic Waves in Layered Media, Cambridge University Press.
- Borgomano, J., Pimienta, L., Fortin, J. & Guéguen, Y., 2017. Dispersion and attenuation measurements of the elastic moduli of a dual-porosity limestone, *J. Geophys. Res.: Solid Earth*, **122**(4), 2690–2711.
- Brocher, T.M., 2005. Empirical relations between elastic wavespeeds and density in the earth's crust, *Bull. Seism. Soc. Am.*, 95(6), 2081–2092.
- Cadoret, T., Marion, D. & Zinszner, B., 1995. Influence of frequency and fluid distribution on elastic wave velocities in partially saturated limestones, J. Geophys. Res.: Solid Earth, 100(B6), 9789–9803.
- Caputo, M., 1967. Linear models of dissipation whose Q is almost frequency independent–II, Geophys. J. Int., 13(5), 529–539.
- Caputo, M., Carcione, J.M. & Cavallini, F., 2011. Wave simulation in biologic media based on the Kelvin-Voigt fractional-derivative stress-strain relation, *Ultrasound Med. Biol.*, 37(6), 996–1004.
- Carcione, J.M., 2007. Wave fields in real media: wave propagation in anisotropic, anelastic, porous and electromagnetic media, in *Handbook of Geophysical Exploration: Seismic Exploration*, Elsevier Science, 81–99.
- Carcione, J.M., Kosloff, D. & Kosloff, R., 1988. Wave propagation simulation in a linear viscoelastic medium, *Geophys. J. Int.*, 95(3), 597–611.
- Carcione, J.M., Cavallini, F., Mainardi, F. & Hanyga, A., 2002. Time-domain modeling of constant-Q seismic waves using fractional derivatives, *Pure Appl. Geophys.*, 159(7–8), 1719–1736.
- Dobrin, M.B. & Savit, C.H., 1988. *Introduction to Geophysical Prospecting*, McGraw-Hill College.
- Dukhin, A.S. & Goetz, P.J., 2009. Bulk viscosity and compressibility measurement using acoustic spectroscopy, *J. Chem. Phys.*, 130(12), 124519, doi.org/10.1063/1.3095471.
- Emmerich, H. & Korn, M., 1987. Incorporation of attenuation into timedomain computations of seismic wave fields, *Geophysics*, 52(9), 1252– 1264.
- Engelberts, W., et al., 1951. Laboratory experiments on the displacement of oil by water from packs of granular material, in 3rd World Petroleum Congress, World Petroleum Congress, https://www.onepetro.org/conference-paper/WPC-4138.
- Feder, J., 1988. Fractals (Physics of Solids and Liquids), Plennum, New York
- Gurevich, B. & Lopatnikov, S., 1995. Velocity and attenuation of elastic waves in finely layered porous rocks, *Geophys. J. Int.*, 121(3), 933–947.
- Hanyga, A., 2003. Anisotropic viscoelastic models with singular memory, J. Appl. Geophys., 54(3-4), 411-425.
- Helle, H.B., Pham, N.H. & Carcione, J.M., 2003. Velocity and attenuation in partially saturated rocks: poroelastic numerical experiments, *Geophys. Prospect.*, 51(6), 551–566.
- Heymans, N. & Bauwens, J.-C., 1994. Fractal rheological models and fractional differential eqs for viscoelastic behavior, *Rheol. Acta*, 33(3), 210–219.
- Holm, S., 2018. Spring–damper equivalents of the fractional, poroelastic, and poroviscoelastic models for elastography, *NMR Biomed.*, 31(10), e3854, doi.org/10.1002/nbm.3854.
- Holm, S., 2019. Waves with Power-Law Attenuation, Springer.
- Jones, W.B. & Thron, W.J., 1980. Continued Fractions: Analytic Theory and Applications (Encyclopedia of Mathematics and Its Applications), Vol. 11, Addison Wesley.
- Kelly, J.F. & McGough, R.J., 2009. Fractal ladder models and power law wave eqs, J. Acoust. Soc. Am., 126(4), 2072–2081.

- Kjartansson, E., 1979. Constant Q-wave propagation and attenuation, J. Geophys. Res.: Solid Earth, 84(B9), 4737–4748.
- Knopoff, L., 1964. Q, Rev. Geophys., 2(4), 625–660, doi.org/10.1029/RG002i004p00625.
- Koeller, R., 1984. Applications of fractional calculus to the theory of viscoelasticity, J. Appl. Mech., 51(2), 299–307.
- Mainardi, F. & Spada, G., 2011. Creep, relaxation and viscosity properties for basic fractional models in rheology, *Eur. Phys. J. Spec. Top.*, 193(1), 133–160.
- McDonal, F., Angona, F., Mills, R., Sengbush, R., Van Nostrand, R. & White, J., 1958. Attenuation of shear and compressional waves in Pierre Shale, *Geophysics*, 23(3), 421–439.
- Metzler, R. & Nonnenmacher, T.F., 2003. Fractional relaxation processes and fractional rheological models for the description of a class of viscoelastic materials, *Int. J. Plast.*, **19**(7), 941–959.
- Molyneux, J.B. & Schmitt, D.R., 2000. Compressional-wave velocities in attenuating media: a laboratory physical model study, *Geophysics*, 65(4), 1162–1167.
- Morozov, I.B. & Deng, W., 2016. Macroscopic framework for viscoelasticity, poroelasticity, and wave-induced fluid flows—part 1: general linear solid, *Geophysics*, 81(1), L1–L13.
- Müller, T.M. & Gurevich, B., 2004. One-dimensional random patchy saturation model for velocity and attenuation in porous rocksradom patchy saturation model, *Geophysics*, **69**(5), 1166–1172.
- Müller, T.M. & Gurevich, B., 2005. A first-order statistical smoothing approximation for the coherent wave field in random porous media, J. Acoust. Soc. Am., 117(4), 1796–1805.
- Müller, T.M., Toms-Stewart, J. & Wenzlau, F., 2008. Velocity-saturation relation for partially saturated rocks with fractal pore fluid distribution, *Geophys. Res. Lett.*, 35(9), doi.org/10.1190/1.2792806.
- Müller, T.M., Gurevich, B. & Lebedev, M., 2010. Seismic wave attenuation and dispersion resulting from wave-induced flow in porous rocks—a review, *Geophysics*, 75(5), 75A147–75A164.
- Näsholm, S.P. & Holm, S., 2011. Linking multiple relaxation, power-law attenuation, and fractional wave eqs, J. Acoust. Soc. Am., 130(5), 3038– 3045.
- Näsholm, S.P. & Holm, S., 2013. On a fractional Zener elastic wave equation, Fract. Calculus Appl. Anal., 16(1), 26–50.
- Picotti, S. & Carcione, J.M., 2017. Numerical simulation of wave-induced fluid flow seismic attenuation based on the Cole-Cole model, *J. Acoust. Soc. Am.*, 142(1), 134–145.
- Pride, S.R. & Masson, Y.J., 2006. Acoustic attenuation in self-affine porous structures, *Phys. Rev. Lett.*, 97(18), 184301.
- Sams, M., Neep, J., Worthington, M. & King, M., 1997. The measurement of velocity dispersion and frequency-dependent intrinsic attenuation in sedimentary rocks, *Geophysics*, 62(5), 1456–1464.
- Schiessel, H. & Blumen, A., 1993. Hierarchical analogues to fractional relaxation equations, *J. Phys. A: Math. Gen.*, **26**(19), 5057, doi: 10.1088/0305-4470/26/19/034.
- Scott-Blair, G.W., 1949. Survey of General and Applied Rheology, Sir Isaac Pitman & Sons.
- Shapiro, S.A. & Müller, T.M., 1999. Seismic signatures of permeability in heterogeneous porous media, *Geophysics*, **64**(1), 99–103.
- Sidler, R., Rubino, J.G. & Holliger, K., 2013. Quantitative comparison between simulations of seismic wave propagation in heterogeneous poroelastic media and equivalent visco-elastic solids for marine-type environments, *Geophys. J. Int.*, 193(1), 463–474.
- Stankiewicz, A., 2018. Fractional Maxwell model of viscoelastic biological materials, in BIO Web of Conferences, Vol. 10, p. 02032, EDP Sciences.
- Strick, E., 1984. Implications of Jeffreys-Lomnitz transient creep, J. Geophys. Res.: Solid Earth, 89(B1), 437–451.
- Strick, E. & Mainardi, F., 1982. On a general class of constant-Q solids, Geophys. J. R. astr. Soc., 69(2), 415–429.
- Toms, J., Müller, T., Ciz, R. & Gurevich, B., 2006. Comparative review of theoretical models for elastic wave attenuation and dispersion in partially saturated rocks, *Soil Dyn. Earthq. Eng.*, 26(6–7), 548–565.
- Toms, J., Müller, T.M. & Gurevich, B., 2007. Seismic attenuation in porous rocks with random patchy saturation, *Geophys. Prospect.*, **55**(5), 671–678.

- Wang, Z., Schmitt, D.R. & Wang, R., 2017. Modeling of viscoelastic properties of nonpermeable porous rocks saturated with highly viscous fluid at seismic frequencies at the core scale, *J. Geophys. Res.: Solid Earth*, 122(8), 6067–6086.
- White, J., 1975. Computed seismic speeds and attenuation in rocks with partial gas saturation, *Geophysics*, **40**(2), 224–232.
- White, J.E., Mihailova, N. & Lyakhovitsky, F., 1975. Low-frequency seismic waves in fluid-saturated layered rocks, J. Acoust. Soc. Am., 57(S1), S30–S30.
- Wuenschel, P.C., 1965. Dispersive body waves—an experimental study, Geophysics, 30(4), 539–551.
- Xing, G. & Zhu, T., 2019. Modeling frequency-independent Q viscoacoustic wave propagation in heterogeneous media, J. Geophys. Res.: Solid Earth, 124(11), 11568–11584.
- Zhu, T. & Carcione, J.M., 2014. Theory and modelling of constant-Q Pand S-waves using fractional spatial derivatives, *Geophys. J. Int.*, 196(3), 1787–1795.
- Zhu, T. & Harris, J.M., 2014. Modeling acoustic wave propagation in heterogeneous attenuating media using decoupled fractional laplacians, *Geophysics*, 79(3), T105–T116.
- Zhu, T., Harris, J.M. & Biondi, B., 2014. Q-compensated reverse-time migration, Geophysics, 79(3), S77–S87.

APPENDIX A: DERIVATION FOR THE COMPLEX MODULUS OF THE QUASI-FRACTAL LADDER MODEL

The structure of a finite QLM is shown in Fig. 2. Let M_k be the modulus from the node N_k to the bottom. According to the recursive structure, these moduli satisfy the following relations:

$$\frac{1}{M} = \frac{1}{E_1} + \frac{1}{M_1},\tag{A1}$$

$$M_k = i\omega\eta_k + \frac{1}{\frac{1}{E_{k+1}} + \frac{1}{M_{k+1}}}, \qquad (k = 1, 2, 3, \dots, n-2)$$
 (A2)

$$M_{n-1} = i\omega\eta_{n-1} + E_n. \tag{A3}$$

Eq. (A2) can be converted into a recursive form:

$$\frac{E_k}{M_k} = \frac{(i\omega\eta_k)^{-1}E_k}{1+} \frac{(i\omega\eta_k)^{-1}E_{k+1}}{1+} \frac{E_{k+1}}{M_{k+1}}. \qquad (k = 1, 2, 3, \dots, n-2)$$
(A4)

Reshape eq. (A1) into a similar form:

$$\frac{M}{E_1} = \frac{1}{1+\frac{E_1}{M_1}}. (A5)$$

Then plugging eq. (A4) into eq. (A5) recursively yields

$$\frac{M}{E_1} = \frac{1}{1+} \frac{(i\omega\eta_1)^{-1} E_1}{1+} \frac{(i\omega\eta_1)^{-1} E_2}{1+} \frac{(i\omega\eta_2)^{-1} E_2}{1+} \frac{(i\omega\eta_2)^{-1} E_3}{1+} \dots \frac{(i\omega\eta_{n-2})^{-1} E_{n-1}}{1+} \frac{E_{n-1}}{M_{n-1}}.$$
(A6)

Moreover, eq. (A3) can be written as

$$\frac{1}{M_{n-1}} = \frac{(i\omega\eta_{n-1})^{-1}}{1+} \frac{(i\omega\eta_{n-1})^{-1}E_n}{1}.$$
(A7)

Finally, plugging eq. (A7) into eq. (A6) yields

$$\frac{M}{E_1} = \frac{1}{1+} \frac{(i\omega\eta_1)^{-1}E_1}{1+} \frac{(i\omega\eta_1)^{-1}E_2}{1+} \frac{(i\omega\eta_2)^{-1}E_2}{1+} \frac{(i\omega\eta_2)^{-1}E_3}{1+} \dots \frac{(i\omega\eta_{n-1})^{-1}E_{n-1}}{1+} \frac{(i\omega\eta_{n-1})^{-1}E_n}{1}.$$
(A8)

Then, it is straightforward to convert eq. (A8) into eq. (11).

APPENDIX B: REPRESENTATION OF BINOMIAL FUNCTION BY CONTINUED FRACTIONS

A detailed review of continued fraction as well as its properties related to the hypergeometric function can be found in Jones & Thron (1980). The hypergeometric function is defined by

$$F(a,b;c;z) = 1 + \frac{ab}{c} \frac{z}{1!} + \frac{a(a+1)b(b+1)}{c(c+1)} \frac{z^2}{2!} + \dots$$
(B1)

Let a and c be complex constants. A complex sequence $\{a_n\}$ defined by

$$\begin{cases} a_{2n+1} = -\frac{(a+n)(c+n-1)}{(c+2n-1)(c+2n)}, & n = 0, 1, 2, \dots \\ a_{2n} = -\frac{n(c-a+n-1)}{(c+2n-2)(c+2n-1)}, & n = 1, 2, 3, \dots \end{cases}$$
(B2)

satisfies the relation

$$F(a,1;c;z) = \left(1 + \sum_{n=1}^{\infty} \frac{a_n z}{1}\right)^{-1},$$
(B3)

where the continued fraction operator is defined by

$$\sum_{i=1}^{\infty} \frac{a_i}{b_i} = \frac{a_1}{b_1 + \frac{a_2}{b_2 + \frac{a_3}{b_3 + \dots}}} \dots$$
(B4)

The letter 'K' stands for Kettenbruch, the German word for 'continued fraction'. The general binomial function can be represented by a hypergeometric function and so a continued fraction:

$$(1+z)^{\beta} = F(-\beta, 1; 1; -z)$$

$$= \frac{1}{1+} \frac{(-\beta)z}{1+} \frac{1(1+\beta)z}{2+} \frac{1(1-\beta)z}{3+} \frac{2(2+\beta)z}{4+} \frac{2(2-\beta)z}{5+} \dots$$
(B5)

eq. (B5) is then manipulated into eq. (13).

APPENDIX C: GENERALIZED QUASI-FRACTAL LADDER MODEL

Fig. 8 shows the structure of the GOLM. Similar to eq. (12), the infinite GOLM has the following relation:

$$\frac{M}{M_{Y_1}} = \frac{1}{1+} \frac{M_{Y_1}/M_{Z_1}}{1+} \frac{M_{Y_2}/M_{Z_1}}{1+} \frac{M_{Y_2}/M_{Z_2}}{1+} \frac{M_{Y_3}/M_{Z_3}}{1+} \dots, \tag{C1}$$

where M_{Y_k} and M_{Z_k} (k = 1, 2, 3, ...) denote the complex moduli of their corresponding mechanical elements. We would like to achieve the equivalence between eqs (13) and (C1) by making the corresponding terms equal, which yields

$$\frac{M}{M_{Y_1}} = (1+z)^{\beta}.$$
 (C2)

In this model, instead of the z assignment in the main body, we let $z = \frac{b}{(i\omega)^{\epsilon}}$ with $0 < \epsilon < 1$. Hence, for an adequately large b, eq. (C2) approximately yields

$$M(\omega) \approx M_{Y_1} b^{\beta} (i\omega)^{-\epsilon\beta}$$
. (C3)

We consider the situation when $M_{Y_1} \propto (i\omega)^{\delta}$ with $0 < \delta < 1 - \epsilon$. In particular, when M_{Y_1} satisfies

$$M_{Y_1} = M_0 \omega_0^{-2\gamma} b^{-\beta} (i\omega)^{\delta} \tag{C4}$$

with $\beta = \frac{\delta - 2\gamma}{\epsilon}$, eq. (C3) approximates the Kjartansson complex modulus (eq. 1) and the frequency-independent Q behaviour is realized by

As we have mentioned, the GQLM representation requires the equivalence of each pair of corresponding terms in eqs (13) and (C1). This requirement leads to constraints on the complex moduli of the mechanical elements:

$$\frac{M_{Y_1}}{M_{Z_1}} = -\beta z,\tag{C5}$$

$$\frac{M_{Y_k}}{M_Z} = \frac{(k-1)(k-1+\beta)z}{(2k-3)(2k-2)}, \qquad (k=2,3,4\ldots)$$
 (C6)

$$\frac{M_{Y_k}}{M_{Z_{k-1}}} = \frac{(k-1)(k-1+\beta)z}{(2k-3)(2k-2)}, \qquad (k=2,3,4...)$$

$$\frac{M_{Y_k}}{M_{Z_k}} = \frac{(k-1)(k-1-\beta)z}{(2k-2)(2k-1)}. \qquad (k=2,3,4...)$$
(C6)

As a consequence, such requirements can only be met when $\frac{M_{Y_i}}{M_{Z_i}} \propto (i\omega)^{-\epsilon}$ for arbitrary (i,j). Since $M_{Y_1} \propto (i\omega)^{\delta}$, we have $M_{Y_i} \propto (i\omega)^{\delta}$ and $M_{Z_i} \propto (i\omega)^{\delta+\epsilon}$ for arbitrary i and j. Hence, the sequence $\{Y_k\}$ are constant-Q mechanical elements with the same $Q = (\tan(\frac{\pi\delta}{2}))^{-1}$, while the sequence $\{Z_k\}$ have the same $Q = \left(\tan\left(\frac{\pi(\delta + \epsilon)}{2}\right)\right)^{-1}$. Essentially, $\{Y_k\}$ are high Q elements, while $\{Z_k\}$ have lower Q. Note that when δ = 0 and $\epsilon = 1$, the GQLM reduces to the QLM as $\{Y_k\}$ become super-springs with $Q \to \infty$, while $\{Z_k\}$ become super-dashpots with Q = 0.